Spin and Quadrupole Couplings of IMRACs

陈斌

北京大学

ICTS-USTC, 2019 年 4 月 28 日

Based on arXiv: 1901.05370
with G. Compère, Y. Liu(ULB), J. Long(APCTP) and X.A. Zhang(PKU)

IMBH: intermediate-mass black holes

$$M_{BH} \sim 10^2 - 10^5 M_\odot$$

IMBHs could be primordial, generated in the early Universe, or they may form in center of dense globular clusters through runaway stellar collision. They are thought to be the seeds from which SMBHs grow.

Astrophysical problems: galaxy formation and growth, BH accretion and the reionisation ...

Accumulated evidence: X-ray and optical observation

No reliable way to determine its mass and spin

$\Rightarrow$ Gravitational wave?

IMRAC: intermediate mass-ratio coalescence

$$q = \frac{M_{CO}}{M_{BH}} \sim 10^{-2} - 10^{-4}.$$

In the literature, it was often termed intermediate mass-ratio inspiral (IMRI).

IMRAC: intermediate mass-ratio coalescence

$$q = \frac{M_{CO}}{M_{BH}} \sim 10^{-2} - 10^{-4}.$$

In the literature, it was often termed intermediate mass-ratio inspiral (IMRI). Two types of IMRACs:

1. Type I: the stellar mass compact object orbiting around IMBH
2. Type II: IMBH orbiting around a supermassive black hole in the center of galaxies

GW from IMRACs

Depending on their orbital parameters, IMRACs in clusters can be detectable not only by the planned space-based gravitational wave observatories, including LISA, 太极/天琴,..., but also by the ground-based observatories, LIGO/Virgo, KAGRA or ET. Amaro-Seoane 2018, Audley et.al. 2017, Huerta et.al. 2011

GW from IMRACs

Depending on their orbital parameters, IMRACs in clusters can be detectable not only by the planned space-based gravitational wave observatories, including LISA, 太极/天琴,..., but also by the ground-based observatories, LIGO/Virgo, KAGRA or ET. Amaro-Seoane 2018, Audley et.al. 2017, Huerta et.al. 2011

In particular, for IMRACs with a total mass $\leq 2000 M_{\odot}$ and initial eccentricities up to 0.999 (nearly a circular orbit), the gravitational waves can be detected first by LISA one year in advance such that the ground-based observatories can get a warning. Amaro-Seoane 2018
Event rate: a few hundred per year Gair et.al 2010

GW from IMRACs

Depending on their orbital parameters, IMRACs in clusters can be detectable not only by the planned space-based gravitational wave observatories, including LISA, 太极/天琴,..., but also by the ground-based observatories, LIGO/Virgo, KAGRA or ET. Amaro-Seoane 2018, Audley et.al. 2017, Huerta et.al. 2011

In particular, for IMRACs with a total mass $\leq 2000 M_{\odot}$ and initial eccentricities up to 0.999 (nearly a circular orbit), the gravitational waves can be detected first by LISA one year in advance such that the ground-based observatories can get a warning. Amaro-Seoane 2018
Event rate: a few hundred per year Gair et.al 2010

The second type of IMRAC would be a very loud source in the LISA band. The GW signal may have a large signal-to-noise ratio (SNR) and can be detectable during the end of inspiral without the need for matched filtering Miller et.al. 2004.
Event rate: a few to a few hundred per year Miller et.al. 2004, Gair 2010

GW from IMRACs

Depending on their orbital parameters, IMRACs in clusters can be detectable not only by the planned space-based gravitational wave observatories, including LISA, 太极/天琴,..., but also by the ground-based observatories, LIGO/Virgo, KAGRA or ET. Amaro-Seoane 2018, Audley et.al. 2017, Huerta et.al. 2011

In particular, for IMRACs with a total mass $\leq 2000 M_{\odot}$ and initial eccentricities up to 0.999 (nearly a circular orbit), the gravitational waves can be detected first by LISA one year in advance such that the ground-based observatories can get a warning. Amaro-Seoane 2018
Event rate: a few hundred per year Gair et.al 2010

The second type of IMRAC would be a very loud source in the LISA band. The GW signal may have a large signal-to-noise ratio (SNR) and can be detectable during the end of inspiral without the need for matched filtering Miller et.al. 2004.
Event rate: a few to a few hundred per year Miller et.al. 2004, Gair 2010

Analytic and numerical studies are highly expected ....

Numerical study

For comparable mass binary systems, the inspiral phase could be well modeled by post-Newtonian(PN) theory and numerical relativity.

Numerical study

For comparable mass binary systems, the inspiral phase could be well modeled by post-Newtonian(PN) theory and numerical relativity.

For EMRIs ($q \sim 10^{-6}$), BH perturbation theory (Teukolsky formalism)

Numerical study

For comparable mass binary systems, the inspiral phase could be well modeled by post-Newtonian(PN) theory and numerical relativity.

For EMRIs ($q \sim 10^{-6}$), BH perturbation theory (Teukolsky formalism)

For IMRACs, not very clear! A hybrid approach, PN + Teukolsky formalism
Kludge waveform model Babak et.al. 2006, Huerta et.al. 2008...
However, the kludge waveform model is developed to compute waveform templates rapidly, without a high precision

Numerical study

For comparable mass binary systems, the inspiral phase could be well modeled by post-Newtonian(PN) theory and numerical relativity.

For EMRIs ($q \sim 10^{-6}$), BH perturbation theory (Teukolsky formalism)

For IMRACs, not very clear! A hybrid approach, PN + Teukolsky formalism
Kludge waveform model Babak et.al. 2006, Huerta et.al. 2008...
However, the kludge waveform model is developed to compute waveform templates rapidly, without a high precision

Analytic study?

Analytic study on high spin BH

Consider the case the the central object is a maximally spinning Kerr black hole.

Type I IMRAC: IMBH is a near-extreme BH

Analytic study on high spin BH

Consider the case the the central object is a maximally spinning Kerr black hole.

Type I IMRAC: IMBH is a near-extreme BH

Type II IMRAC: the central object is a Gargantua

Gargantua: the supermassive BH which is nearly maximal spinning K. Thorne "Interstellar"

X-ray observations: 7 out of 22 AGNs are candidates for being high spin BH Brenneman 1309.6334

Analytic study on high spin BH

Consider the case the the central object is a maximally spinning Kerr black hole.

Type I IMRAC: IMBH is a near-extreme BH

Type II IMRAC: the central object is a Gargantua

Gargantua: the supermassive BH which is nearly maximal spinning K. Thorne "Interstellar"

X-ray observations: 7 out of 22 AGNs are candidates for being high spin BH Brenneman 1309.6334

Why a near extreme Kerr BH special?
Enhanced scaling symmetry in the near horizon region.

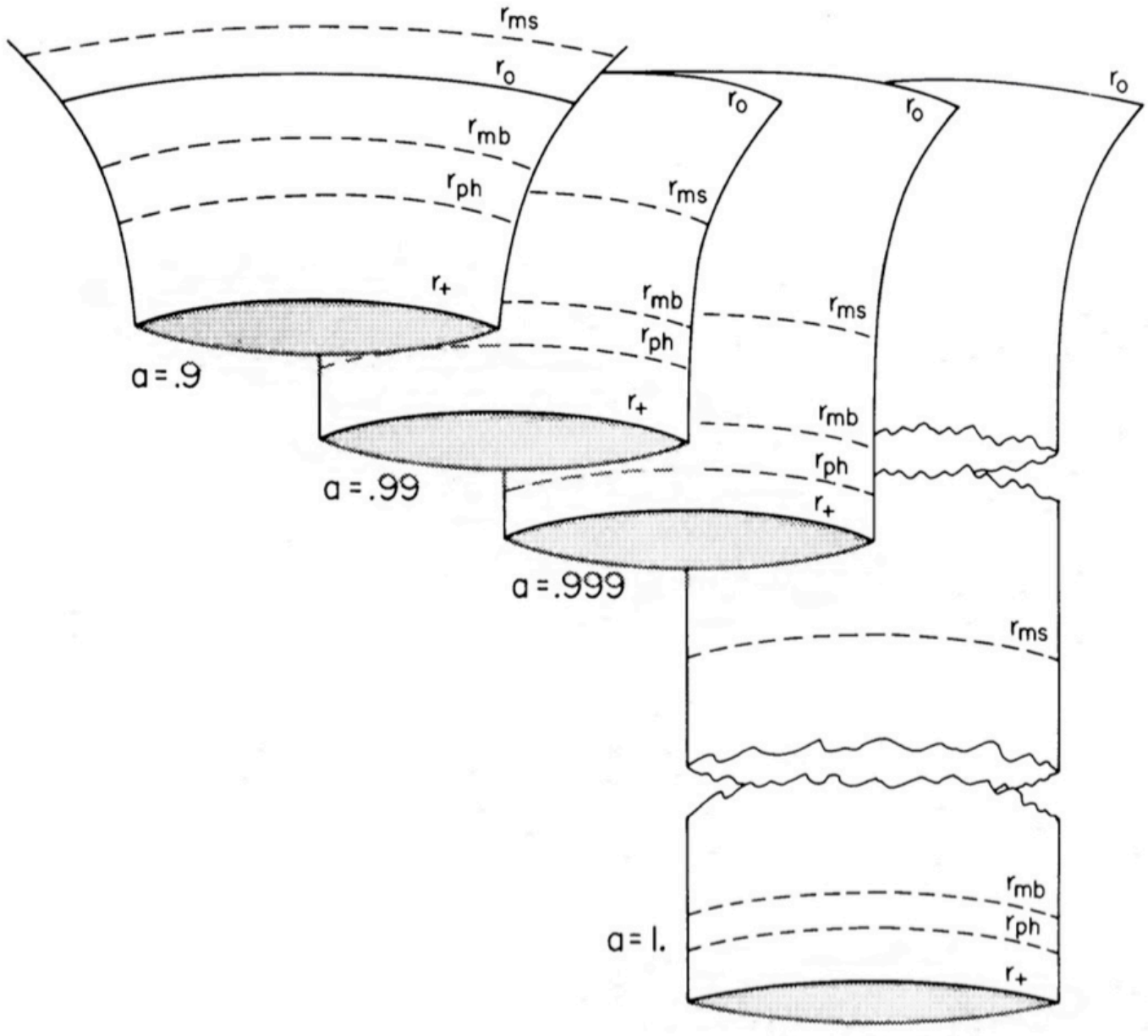

$r_{\mathrm{ms}} = \hat{r}_{\mathrm{ISCO}}$, $r_{\mathrm{mb}} = \hat{r}_{\mathrm{IBCO}}$.

Kerr spacetime

In terms of Boyer-Lindquist coordinates $\hat{t}, \hat{r}, \theta, \hat{\phi}$, the metric of a Kerr spacetime is

$$\begin{aligned} ds^2 &= -(1-\frac{2GM\hat{r}}{\Sigma})d\hat{t} + \frac{\Sigma}{\Delta}d\hat{r}^2 + \Sigma d\theta^2 + \\ &\quad +(\hat{r}^2 + a^2 + \frac{2GMa^2\hat{r}\sin^2\theta}{\Sigma})\sin^2\theta d\hat{\phi}^2 - \frac{4GMa\hat{r}\sin^2\theta}{\Sigma}d\hat{t}d\hat{\phi} \end{aligned}$$

where

$$\Delta \equiv \hat{r}^2 - 2GM\hat{r} + a^2, \qquad \Sigma \equiv \hat{r}^2 + a^2\cos^2\theta,$$

and a is the Kerr parameter $a = J/M$.

For a near extreme Kerr BH, introduce a parameter

$$\lambda = \sqrt{1 - \frac{J^2}{M^4}} << 1.$$

The ISCO and IBCO have different scaling behaviors under $\lambda \to 0$ limit

$$\begin{aligned} \hat{r}_{\text{ISCO}} &= GM + 2^{1/3}\lambda^{2/3}GM + O(\lambda) \\ \hat{r}_{\text{IBCO}} &= GM + 2^{1/2}\lambda GM + o(\lambda). \end{aligned}$$

This motivates us to consider two different limits of near horizon geometry.

NHEK: near horizon geometry of extreme Kerr

Taking the high spin limit $\lambda \to 0$,

$$T = \frac{\hat{t}}{2M}\lambda^{2/3}, \qquad R = \frac{\hat{r} - \hat{r}_+}{M}\lambda^{-2/3}, \qquad \Phi = \hat{\phi} - \frac{\hat{t}}{2M},$$

we get the NEHK geometry J. M. Bardeen and G.T. Horowitz 9905099

$$ds^2 = 2M^2\Gamma(\theta)\left(-R^2 dT^2 + \frac{dR^2}{R^2} + d\theta^2 + \Lambda^2(\theta)(d\Phi + RdT)^2\right),$$

where the polar functions are

$$\Gamma(\theta) = \frac{1 + \cos^2\theta}{2}, \qquad \Lambda(\theta) = \frac{2\sin\theta}{1 + \cos^2\theta}.$$

Obviously it has enhanced $SL(2,\mathbb{R}) \times U(1)$ symmetry.

Near-NHEK: very near horizon region

We may take a different limit: $\lambda \to 0, \kappa$ fixed

$$t = \frac{\hat{t}}{2M\kappa}\lambda, \qquad r = \kappa\frac{\hat{r}-\hat{r}_+}{M\lambda}, \qquad \Phi = \hat{\phi} - \frac{\hat{t}}{2M},$$

we will find the near-NHEK geometry: I. Bredberg et.al. 0907.3477

$$ds^2 = 2M^2\Gamma(\theta)\left(-r(r+2\kappa)dt^2 + \frac{dr^2}{r(r+2\kappa)} + d\theta^2 + \Lambda^2(\theta)(d\phi + (r+\kappa)dt)^2\right),$$

where $\kappa > 0$ is arbitrary as a consequence of emerging scale invariance. The near-NHEK is closer to the horizon than the NHEK. It has enhanced $SL(2,\mathbb{R}) \times U(1)$ symmetry as well.

Besides the enhanced symmetry, there is a discrete PT-symmetry in both NHEK and near-NHEK geometries:

$$T \to -T, \quad \Phi \to -\Phi \quad \text{NHEK}$$
$$t \to -t, \quad \phi \to -\phi \quad \text{near-NHEK}$$

Remarks

The NHEK and near-NHEK has played key roles in setting up the Kerr/CFT correspondence. M. Guica et.al. 0809.4266,I. Bredberg et.al. 0907.3477,BC and C-S Chu 1001.3208

Remarks

The NHEK and near-NHEK has played key roles in setting up the Kerr/CFT correspondence. M. Guica et.al. 0809.4266,I. Bredberg et.al. 0907.3477,BC and C-S Chu 1001.3208

Due to the enhanced symmetry, the motion of the point particles can be classified. It turns out to be that the trajectories in such geometry could be related to each other by conformal transformations and PT transformations. A.P. Porfyriadis and A. Strominger 1401.3746,...

Remarks

The NHEK and near-NHEK has played key roles in setting up the Kerr/CFT correspondence. M. Guica et.al. 0809.4266,I. Bredberg et.al. 0907.3477,BC and C-S Chu 1001.3208

Due to the enhanced symmetry, the motion of the point particles can be classified. It turns out to be that the trajectories in such geometry could be related to each other by conformal transformations and PT transformations. A.P. Porfyriadis and A. Strominger 1401.3746,...

Very recently G. Compere et.al. studied the gravitational wave in the final stages of EMRIs of non-spinning compact objects into supermassive nearly extremal Kerr BH. G. Compere et.al. 1712.0713

- Geodesic approximation: no internal structure of the compact object, no backreaction

Remarks

The NHEK and near-NHEK has played key roles in setting up the Kerr/CFT correspondence. M. Guica et.al. 0809.4266,I. Bredberg et.al. 0907.3477,BC and C-S Chu 1001.3208

Due to the enhanced symmetry, the motion of the point particles can be classified. It turns out to be that the trajectories in such geometry could be related to each other by conformal transformations and PT transformations. A.P. Porfyriadis and A. Strominger 1401.3746,...

Very recently G. Compere et.al. studied the gravitational wave in the final stages of EMRIs of non-spinning compact objects into supermassive nearly extremal Kerr BH. G. Compere et.al. 1712.0713

- Geodesic approximation: no internal structure of the compact object, no backreaction
- Consider GWs at different stages using Teukolsky's formalism: asymp. flat $\Rightarrow$ NHEK $\Rightarrow$ near-NHEK

Remarks

The NHEK and near-NHEK has played key roles in setting up the Kerr/CFT correspondence. M. Guica et.al. 0809.4266,I. Bredberg et.al. 0907.3477,BC and C-S Chu 1001.3208

Due to the enhanced symmetry, the motion of the point particles can be classified. It turns out to be that the trajectories in such geometry could be related to each other by conformal transformations and PT transformations. A.P. Porfyriadis and A. Strominger 1401.3746,...

Very recently G. Compere et.al. studied the gravitational wave in the final stages of EMRIs of non-spinning compact objects into supermassive nearly extremal Kerr BH. G. Compere et.al. 1712.0713

- Geodesic approximation: no internal structure of the compact object, no backreaction
- Consider GWs at different stages using Teukolsky's formalism: asymp. flat $\Rightarrow$ NHEK $\Rightarrow$ near-NHEK
- Paste GWs in different stages

The same treatment can be applied to high spin IMRACs, but ...

Motivation

The small body spin and finite size effect becomes more and more important when the mass-ratio $q > 10^{-3}$.

Motivation

The small body spin and finite size effect becomes more and more important when the mass-ratio $q > 10^{-3}$.

Our recent work is to consider the spin and finite size effect in IMRACs involving a HS BH.

1. The spin effect could be essential in the GW signal emitted from IMRACs if $q \geq 10^{-3}$, by preliminary numerical study Huerta et.al. 2011

2. The finite size effect has not been studied before

3. As the first step for further study in self-force formalism

Beyond point-particle approx.

In the geodesic approximation, the compact object is taken as a point particle without internal structure. This is certainly not true.

This problem has been discussed long time ago, first by M. Mathisson (1937) in an ambitious paper
"Neue mechanik materieller systemes", Acta Phys. Polon **6** (1937)163-2900.
("New mechanics of material systems", Republication, Gen.Rel.Grav. **42**(2010)1011-1048.)

Beyond point-particle approx.

In the geodesic approximation, the compact object is taken as a point particle without internal structure. This is certainly not true.

This problem has been discussed long time ago, first by M. Mathisson (1937) in an ambitious paper
"Neue mechanik materieller systemes", Acta Phys. Polon **6** (1937)163-2900.
("New mechanics of material systems", Republication, Gen.Rel.Grav. **42**(2010)1011-1048.)

Some years later, A. Papapetrou (1951) addressed this issue.
"Spinning test particle in general relativity, 1", Proc. Roy. Soc. Lond. **A209**(1951)248-258.

Beyond point-particle approx.

In the geodesic approximation, the compact object is taken as a point particle without internal structure. This is certainly not true.

This problem has been discussed long time ago, first by M. Mathisson (1937) in an ambitious paper
"Neue mechanik materieller systemes", Acta Phys. Polon **6** (1937)163-2900.
("New mechanics of material systems", Republication, Gen.Rel.Grav. **42**(2010)1011-1048.)

Some years later, A. Papapetrou (1951) addressed this issue.
"Spinning test particle in general relativity, 1", Proc. Roy. Soc. Lond. **A209**(1951)248-258.

The modern version was developed by W.G. Dixon in a series of papers in 1970s. He completed Mathisson's formalism to discuss the dynamics of extended bodies in GR beyond the dipole and quadrupole approx.. This resulted in the so-called Mathisson-Papapetrou-Dixon (MPD) equations.

Mathisson's multipolar scheme

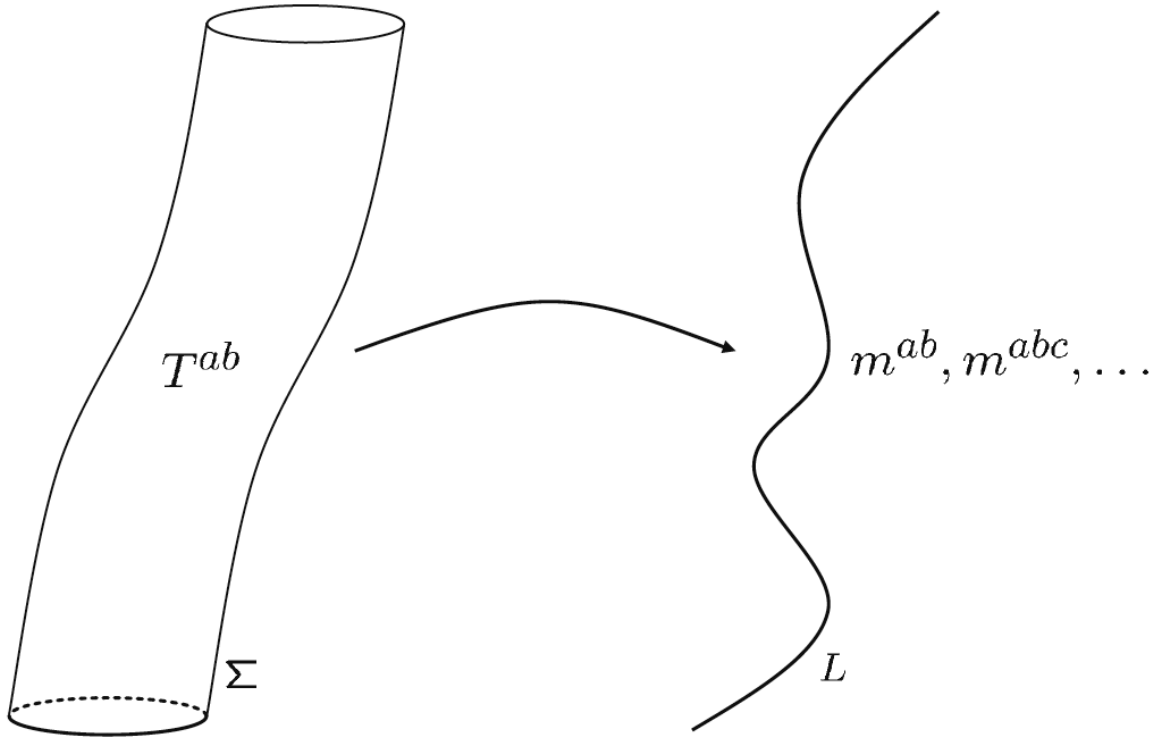

Fig. 1 General idea behind multipolar approximation schemes: The world-tube Σ of a body is replaced by a representative world-line L, whereas the original energy-momentum tensor T^{ab} is substituted by a set of multipole moments $m^{ab\cdots}$ along this world-line. Such a multipolar description simplifies the equations of motion. This is achieved by consideration of only a finite set of moments.

MPD equations

The motion of an extended object could be taken as a world-tube. Relative to the center of mass, there exists an infinite set of moment tensors: momentum p^{μ}, the antisymmetric spin tensor $S^{\alpha\beta}$, together with the quadrupole and higher order moment tensors.

MPD equations

The motion of an extended object could be taken as a world-tube. Relative to the center of mass, there exists an infinite set of moment tensors: momentum p^μ, the antisymmetric spin tensor $S^{\alpha\beta}$, together with the quadrupole and higher order moment tensors.

The MPD evolution equation of the momentum and spin are given by

$$\begin{aligned} \frac{Dp^\mu}{D\tau} &= -\frac{1}{2} R^\mu{}_{\nu\alpha\beta} u^\nu S^{\alpha\beta} + \mathcal{F}^\mu \\ \frac{DS^{\mu\nu}}{D\tau} &= p^\mu u^\nu - p^\nu u^\mu + \mathcal{L}^{\mu\nu} \end{aligned}$$

where $\mathcal{F}^\mu$ and $\mathcal{L}^{\mu\nu}$ are respectively the force and the torque caused by the quadrupole and higher multipoles. The masses $\underline{\mathrm{m}} > 0$, $m > 0$ are defined as

$$\underline{\mathrm{m}}^2 = -p^\mu p_\mu, \qquad m = -p^\mu u_\mu.$$

Note that the 4-momentum cannot simply related to the 4-velocity $p^\mu \neq m u^\mu$.

Moments

The dipole moment is described by the spin tensor $S^{\alpha\beta}$, and the spin length is defined by

$$S^2 = \frac{1}{2} S_{\mu\nu} S^{\mu\nu}.$$

The 2^n-pole moment, $n \geq 2$, is described by a tensor $J^{\mu_1 \cdots \mu_{n-2} \alpha\beta\gamma\delta}$ with $n+2$ indices with the following symmetry structure

$$\begin{aligned}
J^{\mu_1 \cdots \mu_{n-2} \alpha\beta\gamma\delta} &= J^{(\mu_1 \cdots \mu_{n-2})[\alpha\beta][\gamma\delta]}, \\
J^{\mu_1 \cdots \mu_{n-2} \alpha[\beta\gamma\delta]} &= 0, \\
J^{\mu_1 \cdots \mu_{n-3} [\mu_{n-2} \alpha\beta] \gamma\delta} &= 0, \qquad \text{for} \qquad n \geq 3 \\
n_{\mu_1} J^{\mu_1 \cdots \mu_{n-2} \alpha\beta\gamma\delta} &= 0, \qquad \text{for} \qquad n \geq 3
\end{aligned}$$

where $\hat{n}$ is a unit timelike vector.

In particular the quadrupole $J^{\alpha\beta\gamma\delta}$ has 20 independent components and has the symmetries of the Riemann tensor.

Spin supplementary condition (SSC)

The MPD equations are underdetermined. They need to be supplemented by a choice of worldline $x_*^\mu(\tau)$ within the extended body. One can uniquely identify the center-of-mass by imposing $n^\mu = p^\mu/(-p\cdot p)$ together with the Tulczyjew spin supplementary condition

$$S^{\mu\nu}p_\nu = 0.$$

Spin supplementary condition (SSC)

The MPD equations are underdetermined. They need to be supplemented by a choice of worldline $x_*^\mu(\tau)$ within the extended body. One can uniquely identify the center-of-mass by imposing $n^\mu = p^\mu/(-p\cdot p)$ together with the Tulczyjew spin supplementary condition

$$S^{\mu\nu}p_\nu = 0.$$

There are alternative SSCs in the literature. For example the one by Mathisson

$$S^{\mu\nu}u_\nu = 0,$$

however, it does not uniquely fix a worldline already within special relativity.

Quadrupole model

The force and torque caused by the quadrupole $J^{\alpha\beta\gamma\delta}$ is more explicitly given by

$$\begin{aligned} \mathcal{F}^{\mu} &= -\frac{1}{6} J^{\alpha\beta\gamma\delta} \nabla^{\mu} R_{\alpha\beta\gamma\delta}, \\ \mathcal{L}^{\mu\nu} &= \frac{4}{3} J^{\alpha\beta\gamma[\mu} R^{\nu]}{}_{\gamma\alpha\beta}. \end{aligned}$$

For the compact objects, the quadrupole deformation is mainly induced by the spinning

$$J^{\mu\nu\rho\sigma} = 3\kappa_S{}^2 \frac{m}{\underline{m}^4} S^{\alpha[\mu} p^{\nu]} S_{\alpha}{}^{[\rho} p^{\sigma]}.$$

Here we have ignored the quadrupole deformations induced by the gravito-electric and gravito-magnetic tidal fields.

Quadrupole model

The force and torque caused by the quadrupole $J^{\alpha\beta\gamma\delta}$ is more explicitly given by

$$\begin{aligned} \mathcal{F}^{\mu} &= -\frac{1}{6} J^{\alpha\beta\gamma\delta} \nabla^{\mu} R_{\alpha\beta\gamma\delta}, \\ \mathcal{L}^{\mu\nu} &= \frac{4}{3} J^{\alpha\beta\gamma[\mu} R^{\nu]}{}_{\gamma\alpha\beta}. \end{aligned}$$

For the compact objects, the quadrupole deformation is mainly induced by the spinning

$$J^{\mu\nu\rho\sigma} = 3\kappa_{S^2} \frac{m}{\mathrm{m}^4} S^{\alpha[\mu} p^{\nu]} S_{\alpha}^{\ [\rho} p^{\sigma]}.$$

Here we have ignored the quadrupole deformations induced by the gravito-electric and gravito-magnetic tidal fields. The parameters κ_{S^2} characterizes the spin-induced quadrupole

$$\kappa_{S^2} = 1 \ \ (\text{BH}), \qquad \kappa_{S^2} \simeq 5 \ \ (\text{Neutron star}).$$

Strategy

We consider IMRAC with a mass ratio

$$q \equiv \frac{\mu}{M} \ll 1.$$

The probe object has a spin restricted by the extremal black hole bound such that

$$\chi \equiv \frac{S}{\mu^2} \quad \text{obeys} \quad -1 \leq \chi \leq 1$$

Strategy

We consider IMRAC with a mass ratio

$$q \equiv \frac{\mu}{M} \ll 1.$$

The probe object has a spin restricted by the extremal black hole bound such that

$$\chi \equiv \frac{S}{\mu^2} \quad \text{obeys} \quad -1 \leq \chi \leq 1$$

Strategy:
1. Solve the MPD equations with spin and quadrupole in the NHEK and near-NHEK regions

Strategy

We consider IMRAC with a mass ratio

$$q \equiv \frac{\mu}{M} \ll 1.$$

The probe object has a spin restricted by the extremal black hole bound such that

$$\chi \equiv \frac{S}{\mu^2} \quad \text{obeys} \quad -1 \leq \chi \leq 1$$

Strategy:
1. Solve the MPD equations with spin and quadrupole in the NHEK and near-NHEK regions
2. Find the stress tensor of the extended object, which is the source of GW

Strategy

We consider IMRAC with a mass ratio

$$q \equiv \frac{\mu}{M} \ll 1.$$

The probe object has a spin restricted by the extremal black hole bound such that

$$\chi \equiv \frac{S}{\mu^2} \quad \text{obeys} \quad -1 \leq \chi \leq 1$$

Strategy:
1. Solve the MPD equations with spin and quadrupole in the NHEK and near-NHEK regions
2. Find the stress tensor of the extended object, which is the source of GW
3. Solve the Teukolsky problem to read the waveform

The circular near-NHEK trajectory

The circular near-NHEK equatorial trajectory is

$$r = r_0, \qquad \theta = \frac{\pi}{2}, \qquad \phi = -\alpha r_0 t$$

where α is the rescaled angular velocity. The normalization condition $u^2 = -1$ solved for

$$u^t = \frac{1}{M r_0 \sqrt{8(1+\kappa_0)\alpha - (3 + 4\alpha^2 + 6\kappa_0 + 4\kappa_0^2)}}, \qquad u^\phi = -\alpha r_0 u^t,$$

where we defined $\kappa_0 \equiv \frac{\kappa}{r_0}$. Setting $\kappa_0 = 0$, we get the trajectory in NHEK geometry.

Solution to the MPD eq.

Assuming the SSC and using the probe mass μ and spin ratio χ, we obtain the near-NHEK solution to the MPD equations

$$
\begin{aligned}
S^{tr} &= \frac{\ell\chi q^2}{\sqrt{3}\ell_*}(1+2\chi q)+O(q^4),\\
S^{r\phi} &= -\frac{e\chi q^2}{\sqrt{3}\ell_*}(1+\frac{2\chi q}{1-\frac{\ell_*^2}{\ell^2}})+O(q^4),\\
p^t &= -\frac{\sqrt{3}\ell_* q}{2e}(\frac{\ell^2}{\ell_*^2}-1)(1-\frac{\chi^2 q^2}{2})+O(q^4),\\
p^\phi &= -\frac{\sqrt{3}\ell q}{2\ell_*}(1+(\frac{1}{2}-\kappa_{S^2})\chi^2 q^2)+O(q^4),\\
\underline{\mathrm{m}} &= Mq(1-\frac{\kappa_{S^2}}{2}(\frac{\ell^2}{\ell_*^2}+1)\chi^2 q^2)+O(q^4),\\
\frac{\alpha}{\kappa_0} &= \frac{\sqrt{3}\ell}{2\sqrt{\ell^2-\ell_*^2}}(1+\frac{1}{2}(\kappa_{S^2}-1)\chi^2 q^2)+O(q^3).
\end{aligned}
$$

where e and ℓ are specific energy and angular momentum, and ℓ_*

$$\ell_*[\chi q]\equiv\frac{2M}{\sqrt{3}}(1+\chi q+(\frac{1}{2}-\kappa_{S^2})(\chi q)^2)+O(q^3).$$

Stress tensor

The MPD equations are equivalent to the conservation equations $\nabla_\nu T^{\mu\nu} = 0$ of the stress-energy tensor described by the multipole moments.
In the quadrupole approximation, the stress tensor is given by J. Steinhoff and D. Puetzfeld 2009

$$\begin{aligned} T^{\mu\nu} &= \int d\tau [(p^{(\mu} u^{\nu)}) \mathcal{D} + \frac{1}{3} R_{\alpha\beta\gamma}{}^{(\mu} J^{\nu)\gamma\beta\alpha} \mathcal{D} - \nabla_\alpha (S^{\alpha(\mu} u^{\nu)} \mathcal{D}) \\ &\quad - \frac{2}{3} \nabla_\alpha \nabla_\beta (J^{\alpha(\mu\nu)\beta} \mathcal{D})], \end{aligned}$$

where $\mathcal{D}$ is the Dirac function

$$\mathcal{D} = \frac{1}{\sqrt{-g}} \delta^{(4)}(x^\mu - x^\mu_*(\tau)).$$

Stress tensor

The MPD equations are equivalent to the conservation equations $\nabla_\nu T^{\mu\nu} = 0$ of the stress-energy tensor described by the multipole moments.
In the quadrupole approximation, the stress tensor is given by J. Steinhoff and D. Puetzfeld 2009

$$\begin{aligned} T^{\mu\nu} &= \int d\tau[(p^{(\mu}u^{\nu)})\mathcal{D} + \frac{1}{3}R_{\alpha\beta\gamma}{}^{(\mu}J^{\nu)\gamma\beta\alpha}\mathcal{D} - \nabla_\alpha(S^{\alpha(\mu}u^{\nu)}\mathcal{D}) \\ &\quad -\frac{2}{3}\nabla_\alpha\nabla_\beta(J^{\alpha(\mu\nu)\beta}\mathcal{D})], \end{aligned}$$

where $\mathcal{D}$ is the Dirac function

$$\mathcal{D} = \frac{1}{\sqrt{-g}}\delta^{(4)}(x^\mu - x^\mu_*(\tau)).$$

With the MPD solutions, we can read the stress tensor of the extended object straightforwardly.

Teukolsky problem

We consider a source within the NHEK or the near-NHEK region. Within either of these regions, gravitational waves have a frequency $\hat{\omega} \in \mathbb{R}$ and mode number $m \in \mathbb{Z}$ close to the superradiant bound

$$M|\hat{\omega} - \frac{m}{2M}| \ll 1.$$

Teukolsky problem

We consider a source within the NHEK or the near-NHEK region. Within either of these regions, gravitational waves have a frequency $\hat{\omega} \in \mathbb{R}$ and mode number $m \in \mathbb{Z}$ close to the superradiant bound

$$M|\hat{\omega} - \frac{m}{2M}| \ll 1.$$

At the leading order in the high spin limit, the Teukolsky perturbation can be deduced from a matched asymptotic expansion scheme. The details can be found in G. Compère et.al. 1712.07130.

The main quantity of interest is the Newman-Penrose scalar $\delta\psi_4$ defined in the Kinnersley tetrad adapted to the Kerr geometry.

For a source in the NHEK region, $\delta\psi_4$ asymptotes to

$$\delta\psi_4(\hat{r}\to\infty) = \frac{M^3}{\sqrt{2\pi}}\int_{-\infty}^{\infty}\delta\Omega\sum_{lm} B_{lm}(x_*)\mathcal{K}^{far}S_{lm}(\theta)e^{im\hat{\phi}}e^{-\frac{i}{2M}(m+\lambda^{2/3}\Omega)\hat{u}}\hat{r}^{-1}$$

where the asymptotic retarded time $\hat{u} = \hat{t} - \hat{r}^*$ is defined in terms of the asymptotic tortoise coordinate $\hat{r}^*$, $S_{lm}(\theta)$ are the extremal spheroidal harmonics with separation constants $\mathcal{E}_{lm} = l(l+1) + O(m)$, and $\mathcal{K}^{far}$ is fixed.

The coefficients $B_{lm}(x_*)$ encode the details of the source. It is determined by the homogeneous solution to the radial Teukolsky differential equation. The details can be found in the paper.

Metric perturbation

The metric perturbation is related to the curvature perturbation as

$$\delta\psi_4 \to \frac{1}{2}\partial_{\hat{t}}^2(h_+ - ih_\times), \qquad \hat{r} \to \infty.$$

Since the oscillation timescale is locked at $\hat{\omega} = m/(2M)$ at the leading order in λ, we can directly integrate for each mode m to get

$$h_+ - ih_\times = -8(M^2/m^2)\delta\psi_4.$$

The metric perturbation at infinity is therefore given by

$$h_+ - ih_\times = \frac{\mu}{\hat{r}} \sum_{l,m} \mathcal{A}_{lm}(\frac{\ell}{\ell_*}, \chi q; \lambda, \kappa_{S^2}) S_{lm}(\theta) e^{im\hat{\phi} - i\hat{\omega}\hat{u}}$$

where $\mu = qM$ and $\mathcal{A}_{lm} = -8\frac{M^4}{qm^2} B_{lm}(x_*)\mathcal{K}_\kappa^{far}$ is independent of M.

Frequency shift

The frequency of emitted gravitational waves is locked by the kinematics to be around the extremal value

$$\hat{\omega}_{ext} = \frac{m}{2M}.$$

Frequency shift

The frequency of emitted gravitational waves is locked by the kinematics to be around the extremal value

$$\hat{\omega}_{ext} = \frac{m}{2M}.$$

For a circular orbit in NHEK and in the high spin limit, the frequency is given by

$$\frac{\hat{\omega} - \hat{\omega}_{ext}}{\hat{\omega}_{ext}} = -\frac{3\lambda^{2/3}}{2^{5/3}}(1 - \chi q + (\kappa_{S^2} - \frac{5}{4})\chi^2 q^2 + O(q^3)).$$

We observe that a positive secondary spin tends to slightly lower this relative shift.

Frequency shift

The frequency of emitted gravitational waves is locked by the kinematics to be around the extremal value

$$\hat{\omega}_{ext} = \frac{m}{2M}.$$

For a circular orbit in NHEK and in the high spin limit, the frequency is given by

$$\frac{\hat{\omega} - \hat{\omega}_{ext}}{\hat{\omega}_{ext}} = -\frac{3\lambda^{2/3}}{2^{5/3}}(1 - \chi q + (\kappa_{S^2} - \frac{5}{4})\chi^2 q^2 + O(q^3)).$$

We observe that a positive secondary spin tends to slightly lower this relative shift.

For a circular orbit in near-NHEK, the relative shift of angular frequency is

$$\frac{\hat{\omega} - \hat{\omega}_{ext}}{\hat{\omega}_{ext}} = -\frac{\sqrt{3}}{2}\frac{\lambda}{\sqrt{1 - \frac{\ell_*^2}{\ell^2}}}(1 + \frac{1}{2}(\kappa_{S^2} - 1)\chi^2 q^2) + O(q^3).$$

Critical behavior

The description of the near-NHEK orbit displays a critical behavior in the limit $\ell \to \ell_*$ G. Compère et.al. 1712.07130

$$\ell_*[\chi q] \equiv \frac{2M}{\sqrt{3}}(1 + \chi q + (\frac{1}{2} - \kappa_{S^2})(\chi q)^2) + O(q^3)$$

Question: whether the enhancement factor

$$\frac{1}{\sqrt{1 - \frac{\ell_*^2}{\ell^2}}}$$

may actually lead to divergences?

Answer: no!

Because that the near-NHEK approximation requires that

$$\frac{\lambda}{\sqrt{1 - \frac{\ell_*^2}{\ell^2}}} \ll 1.$$

Therefore, the critical behavior $\ell \to \ell_*$ is never exactly reached for a given near-extremality parameter λ.

Amplitude

The leading contribution to the amplitude is[M. Kesden, 1101.3749, S. Gralla et.al. 1506.08496, M. Colleoni et.al. 1501.07330]

$$\mathcal{A} \sim \sqrt{\lambda}.$$

For the near-NHEK circular orbit, we observe that the amplitude displays the following critical behavior

$$\lim_{\ell \to \ell_*} \mathcal{A}_{lm}\left(\frac{\ell}{\ell_*}, \chi q, \lambda, \kappa_{S^2}\right) \sim \left(\frac{\lambda}{\sqrt{1-\frac{\ell_*^2}{\ell^2}}}\right)^{1/2}.$$

The interpretation of this critical behavior is therefore that there is an amplitude enhancement with a power law behavior $\sim (1-\frac{\ell_*^2}{\ell^2})^{-1/4}$ that partially compensate the redshift of the amplitude $\sim \sqrt{\lambda}$ due to the existence of the NHEK region. The final amplitude is always finite.

Ringdown

The ringdown has particular features in the high spin regime.

- The spectrum of quasi-normal modes splits in the near-extremal limit into damped modes in the asymptotically flat region, and into zero-damped modes in the near-horizon region[H. Yang et.al. 1212.3271]

Ringdown

The ringdown has particular features in the high spin regime.

- The spectrum of quasi-normal modes splits in the near-extremal limit into damped modes in the asymptotically flat region, and into zero-damped modes in the near-horizon region H. Yang et.al. 1212.3271
- The presence of zero-damped modes in the near-horizon region leads to polynomial quasi-normal mode ringing due to harmonic stacking of overtones H. Yang et.al. 1307.8086

Ringdown

The ringdown has particular features in the high spin regime.

- The spectrum of quasi-normal modes splits in the near-extremal limit into damped modes in the asymptotically flat region, and into zero-damped modes in the near-horizon region H. Yang et.al. 1212.3271
- The presence of zero-damped modes in the near-horizon region leads to polynomial quasi-normal mode ringing due to harmonic stacking of overtones H. Yang et.al. 1307.8086
- This polynomial ringing gets emitted for geodesic plunges and leads to a "smoking gun" signature of the gravitational wave emission from a plunging source into a high spin black hole G. Compère et.al. 1712.07130, S.Gralla et.al. 1804.04753

These features are identical after finite size corrections, since the angular dependence of the waveform remains unchanged.

Conclusion

We derived the Teukolsky perturbation at leading order in the high spin regime of a finite size compact object orbiting a circular equatorial orbit in the near-horizon region of a highly spinning massive black hole, by solving the MPD equations.

Conclusion

We derived the Teukolsky perturbation at leading order in the high spin regime of a finite size compact object orbiting a circular equatorial orbit in the near-horizon region of a highly spinning massive black hole, by solving the MPD equations.

We discussed the spin and quadrupole corrections to the frequency of emission and to the amplitude.

Conclusion

We derived the Teukolsky perturbation at leading order in the high spin regime of a finite size compact object orbiting a circular equatorial orbit in the near-horizon region of a highly spinning massive black hole, by solving the MPD equations.

We discussed the spin and quadrupole corrections to the frequency of emission and to the amplitude.

Finite size effects allow to distinguish black holes from neutron stars in precise gravitational wave observations. In particular, the measurement of κ_{S^2}, the amplitude of the spin induced quadrupole, encodes information about the internal structure of neutron stars.

Outlook

The first and second order self-force?

The orbits outside the equatorial plane?

Next-to-leading order high spin correction?

Thanks for your attention!

Conserved mass

Given any Killing vector $\hat{\xi}$ of the background spacetime, one can define the conserved quantities

$$Q_\xi = \xi_\mu p^\mu + \frac{1}{2} S^{\mu\nu} \nabla_\mu \xi_\nu,$$

even in the presence of higher multipole moments. J. Ehlers and E. Rudolph (1977)

Conserved mass

Given any Killing vector $\hat{\xi}$ of the background spacetime, one can define the conserved quantities

$$Q_\xi = \xi_\mu p^\mu + \frac{1}{2} S^{\mu\nu} \nabla_\mu \xi_\nu,$$

even in the presence of higher multipole moments. J. Ehlers and E. Rudolph (1977)

The masses m, $\underline{\mathrm{m}}$ are non-conserved and differ at $\mathcal{O}(S^3)$ in the spin tensor,

$$m = \underline{\mathrm{m}} + O(S^3).$$

The masslike quantity μ defined as

$$\mu \quad = \quad m + \frac{\kappa S^2}{2m} E_{\mu\nu} S^\mu{}_\alpha S^{\alpha\nu}$$

is conserved up to $\mathcal{O}(S^3)$, where

$$E_{\mu\nu} \quad = \quad \frac{1}{\underline{\mathrm{m}}^2} R_{\mu\rho\nu\sigma} p^\rho p^\sigma.$$